Array Receiver Optics Design for the Submillimeter Array

Yun-Chih Chou and Chao-Te Li

***Abstract*—This study presents the array receiver optics designs for the upgrade of the Submillimeter Array (SMA). 7-pixel configurations were designed around the key observation frequency of 345 GHz, and the field of view (FOV) increased from 40" to over 5.5'. Five layouts were attempted based on current optics configuration. The optimal solution is a focal plane array (FPA) with 2 off-axis ellipsoidal mirrors in the beam waveguide. Beam efficiencies of both on- and off-axis feeds exceeded 80%, integrated over the far-field beam from peak to 12 dB below, compared with 84% for the current optics.**

***Index Terms*—array receiver, focal plane array, physical optics, quasi-optics, submillimeter wave**

I. Introduction

THE Submillimeter Array (SMA) [1] is a submillimeter interferometer comprising eight 6-meter antennas configurable on baselines ranging from 9 meters to 465 meters. The array is outfitted with Superconductor-Insulator-Superconductor (SIS) mixer receivers [2] [3] housed in a single cryostat to cover atmospheric windows from 176 GHz to 700 GHz. The aim of the SMA is to use interferometric techniques to explore submillimeter wavelengths with high angular resolution. The significance of the submillimeter window derives from the fact that the bulk of the universe is at a relatively cold temperature of approximately 10K, thereby placing the peak of the radiation curve in the submillimeter and far-infrared range. Furthermore, many unique and high excitation molecular lines can become available in the submillimeter window.

As the Atacama Large Millimeter/submillimeter Array (ALMA) is coming online, with its major increase in sensitivity and angular resolution at submillimeter wavelengths, for the SMA upgrade, it has been suggested to remain at the Mauna Kea site and upgrade the array performance, which includes adding array receivers (~7 pixels in a 2-3-2 configuration) to each antenna, improving the sensitivities of the receivers, and increasing the bandwidth of the system to as much as 32 GHz [4]. The importance of running the future SMA to perform large directed key programs, which ALMA may not be able to carry out, was addressed.

Y.-C. Chou and C.-T. Li are with the Institute of Astronomy and Astrophysics, Academia Sinica, Taipei, 10617 Taiwan

II. Array receiver

As the noise performance of radio astronomical instruments approaches the limit set by quantum mechanics or the background, the speed of astronomical observations can only be increased using the imaging capability of the telescope. Radio telescopes, derived from optical designs such as Cassegrain, turn out to have useful fields of view (FOV). Building large format array receivers is a method to exploit these fields to gain mapping speed [5].

In the era of ALMA, an alternative route for other mm/submm telescopes is using array receivers to conduct large surveys of the sky. Direct detectors, such as bolometers, transition edge sensors (TES) and microwave kinetic inductance detectors (MKID), as well as heterodyne receivers, have been adopted in array receiver designs.

Many photometric array receivers exist for ground-based telescopes, balloon-borne experiments, or space missions, for example, Bolocam [6] on CSO, AzTEC [7] and SCUBA-2 [8] on JCMT, LABOCA [9] and APEX-SZ [10] on APEX, MUSTA NG [11] on GBT, as well as bolometer arrays for SPT [12], ASTE [13], EBEX [14], and the Planck Satellite [15]. Arrays also exists that use MKIDs, such as MUSIC [16] for CSO.

Ground-based heterodyne array receivers operating at frequencies ranging from 100GHz to 1 THz include BEARS [17] on NRO, SEQUOIA [18] on LMT, QUARRY [19] on FCRAO, HERA [20] for the IRAM 30m telescope, HARP [21] on JCMT, CHAMP+ [22] on APEX, SMART [23] on NANTEN2, and SSAR [24] on the Delingha 13-m radio telescope. There are some even larger arrays under construction or in development, including the SuperCam [25] for HHT, STO [26], and KAPPa [27]. Groppi published a detailed review of coherent detector arrays [28].

There are challenges for upgrading existing single-pixel telescopes to multi-beam configurations, such as the retrofit of the beam waveguide in the cabin and the aperture diameter limit on the cryostat window. This study presents possible configurations for SMA upgrades from single pixel to 7 pixels for future considerations.

III. SMA optics

Intended for a broadband optical system [29], the design of current SMA optics have adopted the frequency-independent Fresnel imaging approach [30]. Multi-mode Gaussian beam techniques are used as computational tools for solving the propagation of the beam between images [31]. Two focusing mirrors combined with one lens form an imaging beam

waveguide which images the aperture of the receiver feed horn onto the secondary mirror. All bands have the same 10-dB taper illumination on the secondary mirror. Focusing mirrors are common to all receivers, whereas bi-hyperbolic lenses and corrugated feeds are separately optimized for each receiver band.

The folded Naysmith configuration of the beam waveguide directs the beam from the antenna vertically downward into the receiver optics assembly (Fig. 1). The beam is then split into two orthogonally polarized beams by a diplexer consisting of a polarizing wire grid and a mirror. The two orthogonally polarized beams are directed by the diplexer to a pair of receivers. Pair receivers with overlapping frequency bands permit dual polarization observations. Currently the frequency ranges in operation are 200 GHz (176 to 256GHz), 300 GHz (250 to 350 GHz), and 400 GHz (330 to 430 GHz) bands. Dual polarization observations use the 300 GHz and 400 GHz band receivers simultaneously.

The Cassegrain antenna has a focal ratio of 14, and the FOV is 40" at 345 GHz (the key observation frequency). The field scale of the 6-m antenna is 2.45" per millimeter, and the largest possible FOV for a multi-pixel upgrade is 14.3', using the 350mm-in-diameter secondary mirror. The existing SMA optics was optimized for a single-pixel receiver to maintain maximum aperture efficiency and constant spill-over of more than 30% of the bandwidth of each receiver.

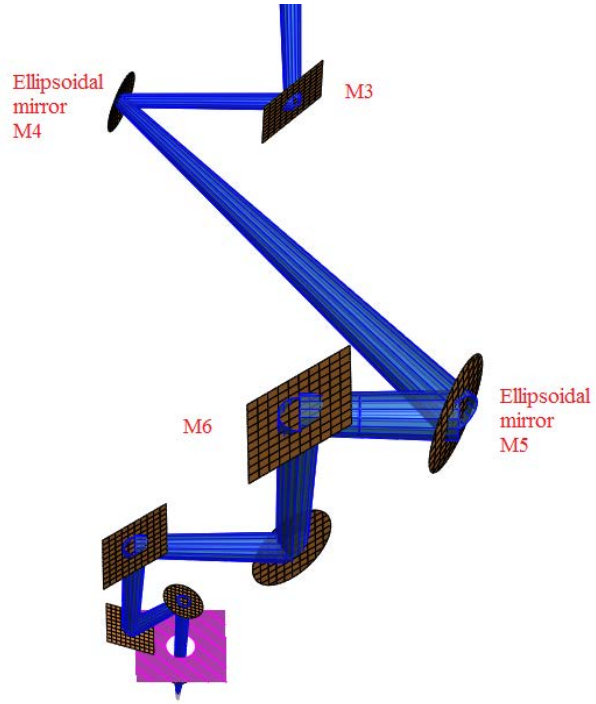

Fig. 1. Model of SMA optics in GRASP. The blue tube illustrates the fundamental Gaussian beam, emitting from the near-field Gaussian beam feed (bottom) to the primary mirror (not shown in the graph). M3 to M6 are the mirrors on the beam waveguide plate. The magenta aperture is the cryostat window. The LO grid and metallic mesh are replaced by flat mirrors.

IV. Design and Simulation

This development started with a 7-pixel array receiver. The feeds were arranged in a hexagonally closed-packed format, with the on-axis feed in the center. The design was centered at the key observation frequency of 345 GHz. The design was aimed to make minimal modifications to the current optics. In addition, focal plane arrays were also considered for the array configuration.

The multi-pixel optics of the SMA was designed using either the frequency-independent imaging method [30] or quasi-optics techniques [32]. The simulation tool used was the reflector optics simulation software GRASP from TICRA (http://www.ticra.com). GRASP is mainly based on physical optics (PO) analysis, supplemented with the physical theory of diffraction (PTD) and other methods [33]. In the simulation model of GRASP a near-field Gaussian beam feed is used with a linear polarization according to Ludwig's third definition [34]. The post-processor of GRASP calculates the beam efficiency of the far-field beam. The beam efficiency (γ) of each polarization is defined by

$$\gamma = \frac{1}{4\pi} \int_{\Omega_0} E_p^2(\Omega) d(\Omega)$$

where Ω_0 is the solid angular region within which the beam efficiency is evaluated, and $E_p(\Omega)$ is the electric field in the polarization direction. The total power radiated by the feed is normalized to 4π [35].

The SMA optics was built in GRASP for comparison with the multi-pixel solutions. The simulation started from the feedhorn to the primary mirror. The far-field E-fields propagating after the primary mirror were recorded. Unless stated otherwise, the beam efficiency referred to in this paper was integrated over the far-field beam from peak to 12 dB below, which takes into account 93% of the power of the beam. In the SMA optics model built in GRASP, wire grids were replaced with flat mirrors (Fig. 1). Fig. 2 shows the result of the far-field radiation patterns after the primary. Figs.3 and 4 show the contour plots of co- and cross-polarization far-field radiations in the El-Az coordinates. The beam efficiency was 83.6%, and the spillover efficiency [36] on the secondary mirror was 96.8% at 345 GHz. Fig. 9 shows the beam efficiency versus frequency.

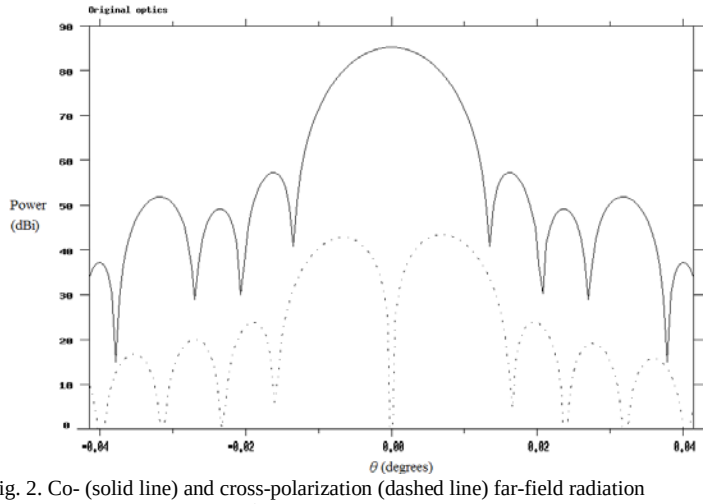

Fig. 2. Co- (solid line) and cross-polarization (dashed line) far-field radiation patterns of SMA optics at 345 GHz

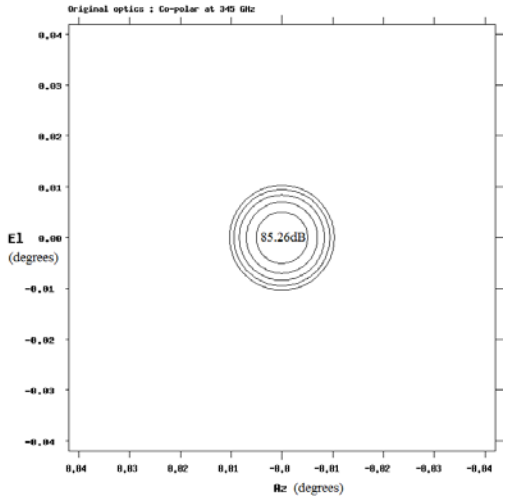

Fig. 3. Contour plot of far-field co-polarization radiation of SMA optics at 345 GHz. Each contour is 3dB apart. The peak value of the beam is also indicated.

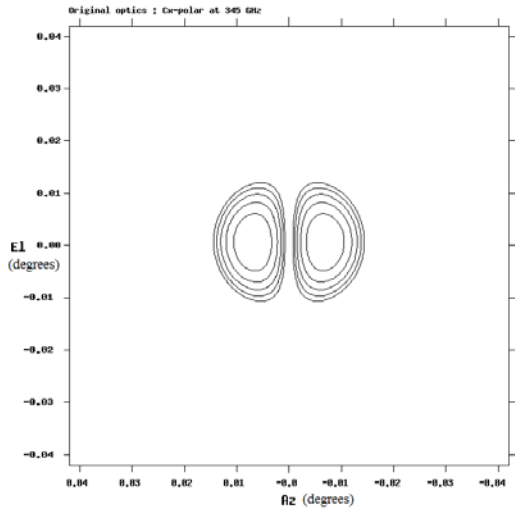

Fig. 4. Contour plot of far-field cross-polarization radiation of SMA optics at 345 GHz. Each contour is 3dB apart. The maximum value is 43.92 dB.

Two layouts based on the current SMA optics were designed. Least change in the receiver cabin was the main concern, and therefore we began by adding the off-axis feeds to form a feed array.

A. Layout 1

Layout 1 maintained the current optics design while adding six off-axis feeds to the central one. The center to center offset was 25mm, accounting for the 76 mm diameter of the cryostat window. The current 70-mm-in-diameter lens was replaced with a 7-lenslet array, each being 25mm in diameter. The 25mm diameter corresponded to 1.8 beam radii, causing great loss because of truncation. The far-field beam efficiency dropped to 57.2% for the on-axis feed, and 40% for the off-axis feeds. This loss resulted from lens truncation and spillover on the secondary mirror. As mentioned, the current design had a 10-dB taper on the secondary rim. When the feed was placed offset to the axis, the spillover on the secondary mirror increased.

B. Layout 2

In layout 2, the optics design was changed and the beam radius was made smaller at the lens. The frequency independent Fresnel imaging technique was used to modify the parameters of the M5, the second ellipsoidal mirror in the beam waveguide. To keep the same optical route as the current one, M5 and the flat mirror M6 were swapped, as listed in Table 1. The drawback was that the incidence angle of M5 increased from 25° to 45°. From the current SMA design, it is shown showed that a larger incidence angle resulted in a smaller coupling efficiency [29].

The 25mm-in-diameter lens equaled the 2.5 beam radii in layout 2. The on-axis beam efficiency improved to 75.2%. However, the beam efficiencies of the off-axis beams were dramatically reduced due to a larger spillover on the secondary reflector. The results of layouts 1 and 2 showed that the current optics was not optimal for the array receiver, and required modification.

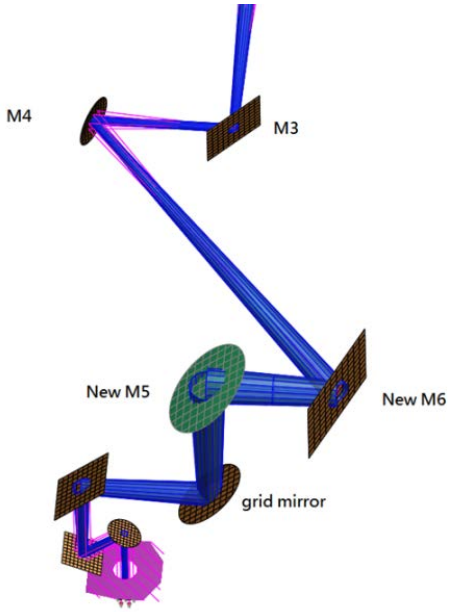

Fig 5. Optics model of layout 2

Table 1 Parameters of the SMA optics and layout 2

Parameters (mm)	**Current Design**	**Layout 2**
Feed position	-88.6	**-34.797**
Feed aperture radius	5.34	**6.438**
Feed slant length (R)	35.65	**25.878**
Lens position	0	0
Lens f	100	**50**
Lens diameter	70	**25**
M6 position	1761	**2161**
M5 position	2161	**1761**
Effective f of M5	726.57	**790**
R1 of M5	1166.9	**1580**
R2 of M5	1925.4	**1580**
M5 incidence angle	24.93 degrees	**45 degrees**
M4 position	3456.6	3456.6
Effective f of M4	309.78	309.78
M4 incidence angle	24.93 degrees	24.93 degrees
Secondary position	8307.2	8307.2

V.FOCAL PLANE ARRAY

In addition, some multi-pixel optics using the FPA configuration is designed. Because the SMA spends considerable observations at 230 and 345 GHz, a straightforward upgrade path to multi pixels is to set the feed at an image of the sky, and optimize the aperture efficiency at these frequencies. That is, a focal plane array may be designed where beams from different off-axis angles are re-imaged to different points in the focal plane. In the following designs, a feed array was placed at the focal plane of the Cassegrain telescope, and relay optics was then added to re-locate the feeds within the cryostat.

A. Layout 3:

Layout 3 added a 7-feed array along with lenses at the Cassegrain focal plane. This layout was a nominal FPA so that all relay optics between the secondary mirror and the lenses were removed. The waist of the feedhorn at 345GHz was placed at the focal point of the lens, whereas the beam waist on the other side of the lens coincided with the focal plane of the Cassegrain.

Regarding the feed spacing, to achieve a fully Nyquist sample of the sky instantaneously, the detector spacing must be 0.5 $F\lambda$, where F is f/D (the focal ratio of the optics). On other hand, beams are typically spaced in the focal plane with a separation of $2F\lambda$, resulting in two-beam spacing on the sky. This yields an optical cross-coupling of approximately -20 dB between elements. This isolation simplifies data processing because signals in adjacent pixels are not correlated, but does require scanning or multiple pointings to create a Nyquist-sampled map [28].

For SMA, the minimum distance between the feeds should be $2F\lambda$ = 24.3 mm at the design frequency of 345 GHz. Feed spacing ranging from 30 mm to 55 mm were simulated using GRASP. The results showed that the off-axis feeds had the highest beam efficiency when the offset, which was also the diameter of the lens, was 45 mm (Table 2). This represented the compromise between the lens truncation and the spillover on the secondary mirror. It was thus necessary to enlarge the cryostat window from 76mm to at least 90 mm in diameter so that all beams were less truncated. The FOV of the 7-feed array is then 5.5'.

The on-axis feed had a 26dB edge taper illumination on the secondary mirror. Fig. 6 shows the far-field radiation patterns of the on-axis beam. Figs.7 and 8 show the contour plots of co- and cross-polarization far-field radiations in the El-Az coordinates. The beam efficiency at 345 GHz was 84.5% for the on-axis beam, and 83.9% for the off-axis beams, excluding cryostat window truncation. The spillover efficiencies of the secondary mirror were 92.7% for the on-axis feed, and 91.8% for the off-axis feeds. Fig. 9 shows the on-axis beam efficiencies at different frequencies. Fig. 10 shows the off-axis beam efficiencies and spillover efficiencies at different frequencies.

Table 2 Feed spacing vs. beam efficiency of layout 3

Feed spacing/ lens diameter (mm)	**Lens diameter in terms of beam radius**	**On-axis beam efficiency (%)**	**Off-axis beam efficiency (%)**	**Off-axis beam overall spillover efficiency (%)**
30/30	2.14	74.1	73.2	80.0
35/35	2.28	80.6	79.7	87.3
40/40	2.84	84.2	83.6	90.7
45/45	**3.2**	**84.5**	**83.9**	**91.8**
50/50	3.56	85.4	83.5	91.8
55/55	3.92	84.6	81.6	91.3

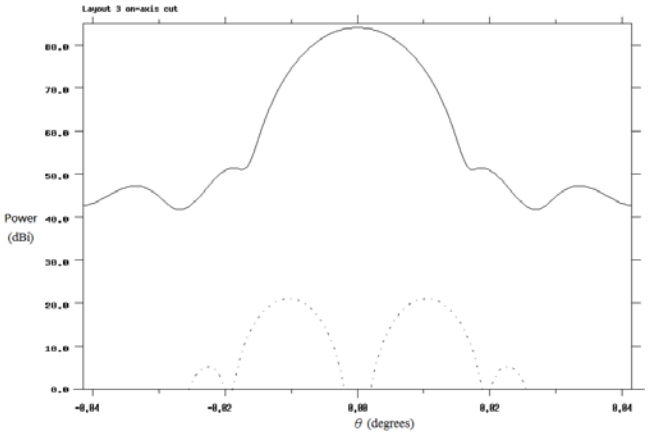

Fig. 6. The on-axis co- (solid line) and cross-polarization (dashed line) far-field radiation patterns of layout 3 at 345 GHz

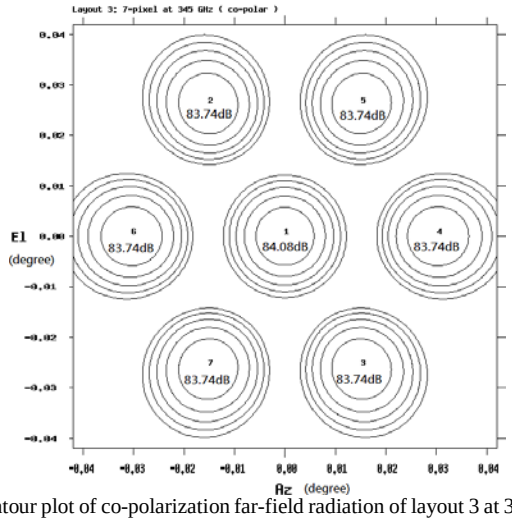

Fig. 7. Contour plot of co-polarization far-field radiation of layout 3 at 345 GHz. Each contour is 3dB apart. The peak value of each beam is also indicated.

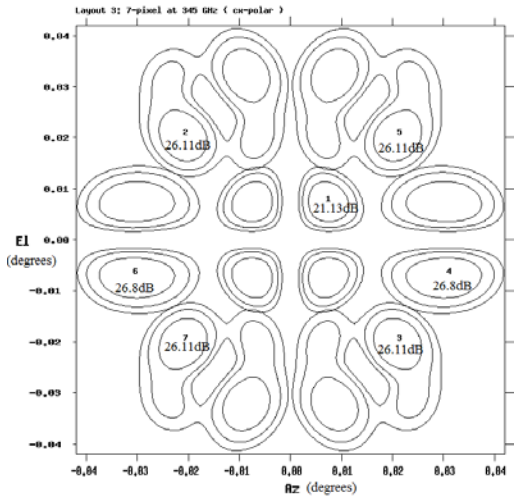

Fig. 8. Contour plot of cross-polarization far-field radiation of layout 3 at 345 GHz. Each contour is 3dB apart. The maximum value of each beam is also indicated.

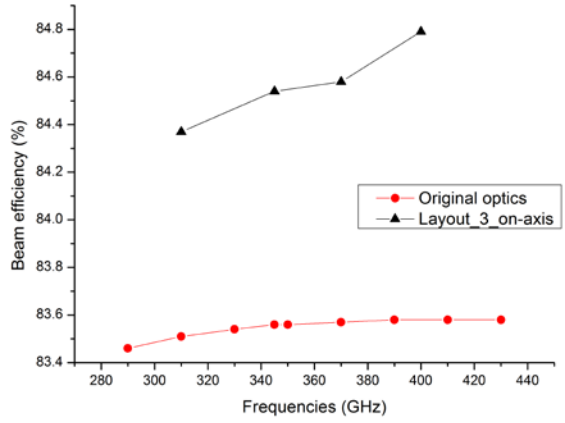

Fig. 9. Beam efficiency of the on-axis beam of the current optics and layout 3 vs. frequency

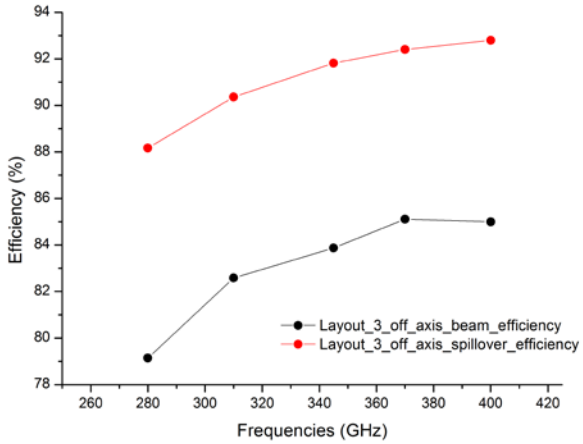

Fig.10. Beam efficiency and spillover efficiency of off-axis beams of layout 3 vs. frequency.

B. Layout 4:

To relay the signals received from the Cassegrain telescope into the cryostat, two warm lenses as the relay optics (RO) were added in layout 4. The advantage of using lenses is that it allows a compact optical path. The lenses form a Gaussian beam telescope [37] and are set identical so that the magnification of the relay optics equals 1. The focal length of the RO lens was set to be 837.6 mm, accounting for the optical path length between the Cassegrain focal plane and the lens/feed array. The diameter of the lens was 200 mm to accommodate 4ω beams at 250 GHz, the lowest frequency of the 300 GHz band. The reflective mirrors in the current optics were replaced with flat mirrors. The first RO lens, which was closer to the feed, was located near the diplexer. The second lens was on the beam waveguide plate (Fig. 11). The rims of the flat mirrors were also enlarged.

Although the lens design made the optics compact and straight-forward, the two warm lenses would contribute to the receiver noise. The beam efficiencies of layout 4 were 74.3% for the on-axis beam, and 73.9% for the off-axis feeds. The overall spillover efficiencies for the on-axis and off-axis feeds were 81% and 80%, respectively.

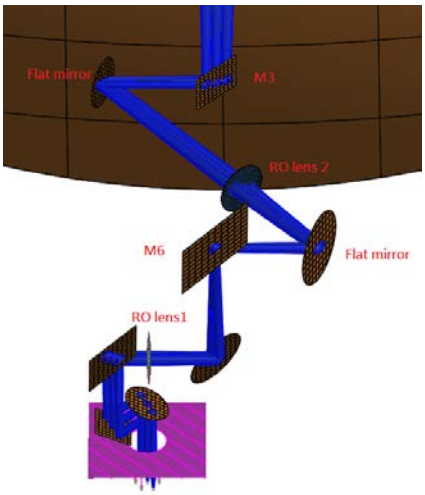

Fig 11. Optics model of layout 4. On-axis and two off-axis Gaussian beams were shown.

C. Layout 5:

In this layout, reflectors were used as the RO focusing elements. Two identical off-axis ellipsoidal mirrors were used to guide the beams. The effective focal lengths were both 837.6 mm, identical to that of the RO lenses in layout 4. The radii of curvature of the incident and reflected phase front, R1 and R2, were set the same for simplicity. The ellipsoidal mirrors were placed in a folded configuration on the beam waveguide plate (Fig. 12). To reduce beam distortion from reflection, the reflection angles of both ellipsoidal mirrors were set identical [37].

The folded configuration of the RO became larger than the current beam waveguide plate. It would be necessary to enlarge the receiver cabin to accommodate the new RO. On the other hand, the distance between the insert lens and the first RO mirror becomes shorter, equal to the sum of the focal lengths of the lens and RO mirror. To achieve this, the turning mirror M6 is placed directly above the array receiver, and the cryostat was lifted by approximately 400 mm.

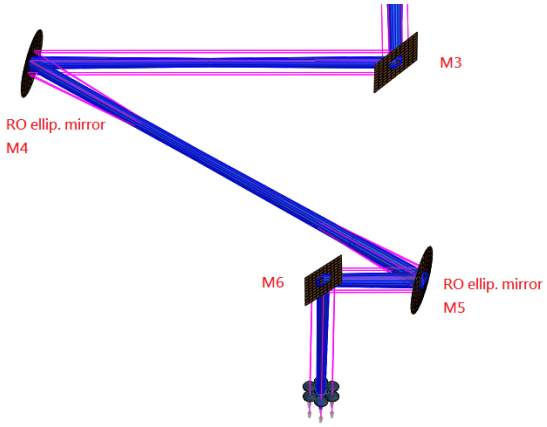

Fig 12. Optics model of layout 5.

At 345GHz, the beam efficiency was 85% for the on-axis beam, and ranged from 80.6% to 84.1% for the off-axis beams. Fig. 13 shows the beam efficiencies versus frequencies for layouts 4 and 5. Fig. 14 shows the off-axis beam efficiency and spillover efficiency versus frequency for layout 5.

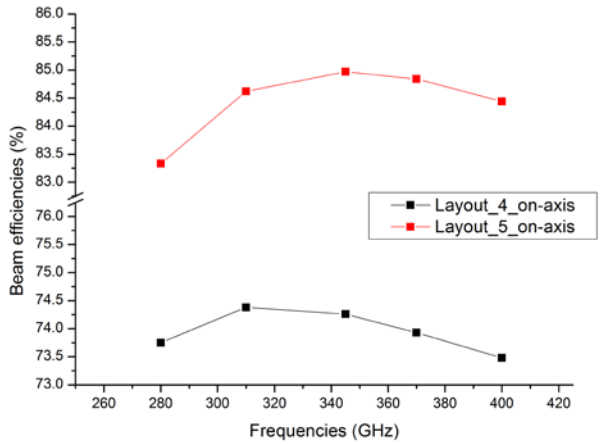

Fig. 13. Beam efficiencies for on-axis beams of layouts 4 and 5 vs. frequency

.

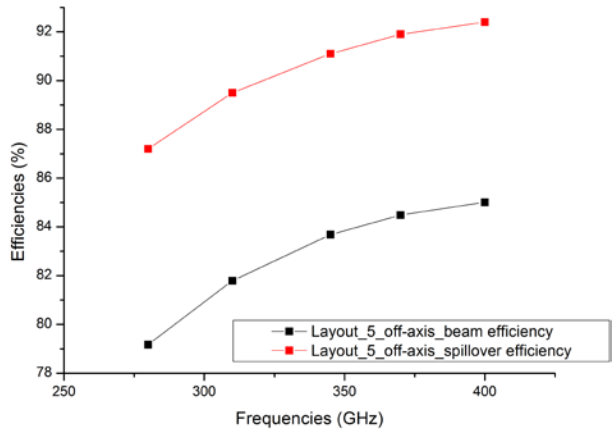

Fig. 14. Beam efficiency and spillover efficiency vs frequency for an off-axis beam of layout 5.

Table 3. Parameters of Layout 3-5

Parameters	Layout 3	Layout 4	Layout 5
Feed position	-88.6 mm		
Feed aperture radius	5.34 mm		
Feed slant length	35.65 mm		
Lens position (on-axis)	0 mm		
Lens f	109.4 mm		
Lens diameter	45 mm		
M6 position		1761 mm	600.69 mm
1st RO position		946.98 mm	
2nd RO position		2622.13 mm	
RO effective f		837.58 mm	
RO R1, R2		737.07 mm	1675.15 mm
M5,M4 reflection angle			36.25 degrees
M3 position		3891.7 mm	
Secondary position	4956.9 mm	8307.2 mm	

REFERENCES

[1] R. Blundell (2007). *Submillimeter Array* [Online]. Available: http://www.cfa.harvard.edu/sma/general/IEEE.pdf

[2] R. Blundell, C.-Y. E. Tong, D. C. Papa, R. L. Leombruno, X. Zhang, S. Paine, J. A. Stern, H. G. LeDuc, and B. Bumble, "A wideband fixed-tuned SIS receiver for 200-GHz operation," *IEEE Trans. Microw. Theory Techn.*, vol. 43, no.4, pp. 933-937, Apr. 1995.

[3] C.-Y. E. Tong, R. Blundell, S. Paine, D. C. Papa, J. Kawamura, X. Zhang, J. A. Stern, and H. G. LeDuc, "Design and characterization of a 250-350-GHz fixed-tuned superconductor-insulator-superconductor receiver," *IEEE Trans. Microw. Theory Techn.*, vol. 44, no.9, pp. 1548-1556, Sep. 1996.

[4] E. Bergin, C. Carilli, G. Fazio, P. Ho, D. Marrone, K. Menten, S. Paine, F. Shu, and G. Stacey (2010, May 12) *Report of the committee on the future of the SMA* [Online]. Available: http://www.cfa.harvard.edu/sma/meetings/Futures/2009/Future_SMA_Comm_10_Ver3.pdf

[5] J. A. Murphy and R. Padman, "Focal-plane and aperture-plane heterodyne array receivers for millimeter-wave radioastronomy - a comparison," *Int. Jour. Infr. Mm. Waves*, vol.9, No. 8, pp. 667-704, 1988.

[6] J. Glenn, J. J. Bock, G. Chattopadhyay, S. F. Edgington, A. E. Lange, and J. Zmuidzinas, "Bolocam: A millimeter-wave bolometric camera," in *Proc. SPIE*, vol. 3357, 1988, pp. 326-334.

[7] G. W. Wilson, J. E. Austermann, T. A. Perera, K. S. Scott, P. A. R. Ade, J. J. Bock, J. Glenn, S. R. Golwala, S. Kim, Y. Kang, D. Lydon, P. D. Mauskopf, C. R. Predmore, C. M. Roberts, K. Souccar, and M. S. Yun, " The AZTEC mm-wavelength camera," *Mon. Not. R. Astron. Soc.*, vol. 386, issue 2, pp. 807-818, 2008.

[8] W. S. Holland, D. Bintley, E. L. Chapin, A. Chrysostomou, G. R. Davis, J. T. Dempsey, W. D. Duncan, M. Fich, P. Friberg, M. Halpern, K. D. Irwin,T. Jenness, B. D. Kelly, M. J. MacIntosh, E. I. Robson, D. Scott, P. A. R. Ade, E. Atad-Ettedgui, D. S. Berry, S. C. Craig, X. Gao, A. G. Gibb, G. C. Hilton, M. I. Hollister, J. B. Kycia, D. W. Lunney, H. McGregor, D. Montgomery, W. Parkes, R. P. J. Tilanus, J. N. Ullom, C. A. Walther, A. J. Walton, A. L. Woodcraft, M. Amiri, D. Atkinson, B. Burger, T. Chuter, I. M. Coulson, W. B. Doriese, C. Dunare, F. Economou, M. D. Niemack, H. A. L. Parsons, C. D. Reintsema, B. Sibthorpe, I. Smail, R. Sudiwala, and H. S. Thomas, " SCUBA-2: the 10 000 pixel bolometer camera on the James Clerk Maxwell Telescope," *Mon. Not. R. Astron. Soc.*, vol. 430, issue 4, pp. 2513-2533, 2013.

[9] G. Siringo, E. Kreysa, A. Kovács, F. Schuller, A. Weiß, W. Esch, H.-P. Gemünd, N. Jethava, G. Lundershausen, A. Colin, R. Güsten, K. M. Menten, A. Beelen, F. Bertoldi, J. W. Beeman, and E. E. Haller, "The large APEX bolometer camera LABOCA," *Astron. Astrophys.*, vol. 497, pp. 945-962, 2009.

[10] D. Schwan, R. Kneissl, P. Ade, K. Basu, A. Bender, F. Bertoldi, H. Böhringer, H.-M. Cho, G. Chon, J. Clarke1, M. Dobbs, D. Ferrusca, D. Flanigan, N. Halverson, W. Holzapfel, C. Horellou, D. Johansson, B. Johnson, J. Kennedy, Z. Kermish, M. Klein, T. Lanting, A. Lee1, M. Lueker, J. Mehl, K. Menten, D. Muders, F. Pacaud, T. Plagge, C.

Reichardt, P. Richards, R. Schaaf , P. Schilke, M. Sommer, H. Spieler, C. Tucker, A. Weiss, B. Westbrook, and O. Zahn, "APEX-SZ: The Atacama Pathfinder Experiment Sunyaev-Zel'dovich instrument, " *Messenger*, vol. 147, pp. 7-12, ESO, Mar. 2012.

[11] S.R. Dicker, P.M. Korngut, B.S. Mason, P.A.R. Ade, J. Aguirre, T.J. Ames,D.J. Benford, T.C. Chen, J.A. Chervenak, W.D. Cotton, M.J. Devlin,E. Figueroa-Feliciano, K.D. Irwin, S. Maher, M. Mello, S.H. Moseley,D.J. Tally, C. Tucker, and S.D. White," MUSTANG: 90 GHz Science with the Green Bank Telescope," in *Proc. SPIE*, vol. 7020, 2008.

[12] E. Shirokoff, B. A. Benson, L. E. Bleem, C. L. Chang, H.-M. Cho, A. T. Crites, M. A. Dobbs, W. L. Holzapfel, T. Lanting, A. T. Lee, M. Lueker, J. Mehl, T. Plagge, H. G. Spieler, and J. D. Vieira, "The South Pole Telescope SZ-Receiver Detectors," *IEEE Tran. Appl. Supercond.*, vol. 19, no. 3, pp. 517-519, Jun. 2009.

[13] T. Takekoshi, T. Minamidani, S.i Nakatsubo, T. Oshima, M. Kawamura, H. Matsuo, T. Sato, N. W. Halverson, A.T. Lee, W. L. Holzapfel, Y. Tamura, A. Hirota, K. Suzuki, T. Izumi, K. Sorai, K. Kohno, and R. Kawabe, "Optics Design and Optimizations of the Multi-Color TES Bolometer Camera for the ASTE Telescope," *IEEE Tran. THz Sci. Technol.*, vol. 2, no. 6, pp. 584-592, Nov. 2012.

[14] B. Westbrook, A. Lee, X. Meng, A. Suzuki, K. Arnold, E. Shirokoff, E. George, F. Aubin, M. Dobbs, K. MacDermid, S. Hanany, K. Raach, A. Aboobaker, J. Hubmayr, T. Oshima, M. Kawamura, and K. Kohno, "Design Evolution of the Spiderweb TES Bolometer for Cosmology Applications," *J. Low Temp. Phys.*, vol.167, issue 5-6, pp. 885–891, Jun. 2012.

[15] M. Piat, J. M. Lamarre, P. A. R. Ade, J. Bock, P. De Bernardis, M. Giard, A. Lange, A. Murphy, J. P. Torre, A. Benoit, R. Bhatia, F. R. Bouchet, B. Maffei, J. L. Puget, R. Sudiwala, and V. Yourchenko, "Use of high sensitivity bolometers on Planck high frequency instrument," in *Infrared, Submillimeter, and Millimeter Detector Working Group*, Monterey, CA, 2002. [Online] Available: http://www.sofia.usra.edu/det_workshop/papers/session5/3-40piat_edjw020613.pdf

[16] J. Sayers, N. G. Czakon, P. K. Day, T. P. Downes, R. P. Duan, J. Gao, J. Glenn, S. R. Golwala, M. I. Hollister, H. G. LeDuc, B. A. Mazin, P. R. Maloney, O. Noroozian, H. T. Nguyen, J. A. Schlaerth, S. Siegel, J. E. Vaillancourt, A. Vayonakis, P. R. Wilson, and J. Zmuidzinas, "Optics for MUSIC: a new (sub)millimeter camera for the Caltech Submillimeter Observatory," in *Proc. SPIE*, vol. 7741, 2010.

[17] C. Yamaguchi, K. Sunada, Y. lizuka, H. Iwashita, and T. Noguchi, "Design of the Focal Plane Array Receiver for the NRO 45.m Telescope," in *Proc. SPIE*, vol. 4015, 2000, pp. 614-623.

[18] G. Narayananl, "Gaussian Beam Analysis of Relay Optics for the SEQUOIA Focal Plane Array," in *Proc.15th Int. Symp. Space THz Techn.*, pp. 406-413, 2004.

[19] N. R. Erickson, P. F. Goldsmith, G. Novak, R. M. Grosslein, P. J. Viscuso, R. B. Erickson, and C. R. Predmore, "A 15 element focal plane array for 100 GHz," *IEEE Trans. Microw. Theory Techn.*, vol. 40, no. 11, pp. 1–11, Jan. 1992.

[20] K.-F. Schuster, C. Boucher, W. Brunswig, M. Carter, J.-Y. Chenu, B. Foullieux, A. Greve, D. John, B. Lazareff, S. Navarro, A. Perrigouard, J.-L. Pollet, A. Sievers, C. Thum, and H. Wiesemeyer, "A 230 GHz heterodyne receiver array for the IRAM 30 m telescope," *Astron. Astrophys.*, vol. 423, pp. 1171–1177, 2004.

[21] H. Smith, J. Buckle, R. Hills, G. Bell, J. Richer, E. Curtis, S. Withington, J. Leech, R. Williamson, W. Dent, P. Hastings, R. Redman, B. Wooff, K. Yeung, P. Friberg, C. Walther, R. Kackley, T. Jenness, R. Tilanus, J. Dempsey, M. Kroug, T. Zijlstra, and T. M. Klapwijk, "HARP: A submillimetre heterodyne array receiver operating on the James Clerk Maxwell Telescope," in *Proc. SPIE*, vol. 7020, 2008, pp. 1–15.

[22] C. Kasemann, S. Heyminck, A. Bell, A. Belloche, C. Castenholz, R. Güsten, H. Hafok, A. Henseler, S. Hochgürtel, B. Klein, T. Klein, I. Krämer, A. Korn, K. Meyer, D. Muders, F. Pacek, F. Schäfer, G. Schneider, G. Wieching, H -J. Wunsch, A. Baryshev, R. Hesper, T. Zijlstra, C. F. J. Lodewijk, and T. M. Klapwijk, "CHAMP+: A powerful submm heterodyne array," in *Proc. 19th Int, Symp. Space THz Techn.*, 2008, pp. 166-172.

[23] U. U. Graf, S. Heyminck, E. A. Michael, S. Stanko, C. E. Honingh, K. Jacobs, R. Schieder, and J. Stutzki, "SMART: The KOSMA sub-millimeter array receiver for two frequencies," in *Proc. 13th Int. Symp. Space THz Techn.*, 2002, pp. 143-152.

[24] W. Shan, J. Yang, S. Shi, Q. Yao, Y. Zuo, Z. Lin, S. Chen, X. Zhang, W. Duan, A. Cao, S. Li, Z. Li, J. Liu, and J. Zhong, "Development of Superconducting Spectroscopic Array Receiver: A multibeam 2SB SIS receiver for millimeter-wave radio astronomy," *IEEE Tran. THz Sci. Technol.*, vol. 2, no. 6, pp. 593-604, Nov. 2012.

[25] C. Groppi, C. Walker, C. Kulesa, D. Golish, J. Kloosterman, S. Weinreb, G. Jones, J. Barden, H. Mani, T. Kuiper, J. Kooi, A. Lichtenberger, T. Cecil, P. Puetz, G. Narayanan, and A. Hedden, "Test and integration results from SuperCam: a 64-pixel array receiver for the 350 GHz atmospheric window," in *Proc. SPIE*, vol. 7741, 2010, pp. 368-373.

[26] C. K. Walker, C. A. Kulesa, C. E. Groppi, E. Young, T. McMahon, P. Bernasconi, C. Lisse, D. Neufeld, D. Hollenbach, J. Kawamura, P. Goldsmith, W. Langer, H. Yorke, J. Sterne, A. Skalare, I. Mehdi, S. Weinreb, J. Kooi, J. Stutzki, U. Graf, C. Honingh, P. Puetz, C. Martin, and M. Wolfire, "The Stratospheric Terahertz Observatory (STO) an LDB experiment to investigate the life cycle of the interstellar medium," in *Proc. 19th Int. Symp. Space THz Techn.*, 2008, pp. 28-32.

[27] C. Groppi, C. Wheeler, H. Mani, S. Weinreb, D. Russell, J. Kooi, A. Lichtenberger, and C. Walker, "The Kilopixel Array Pathfinder Project (KAPPa): A 16 pixel 660 GHz pathfinder instrument with an integrated heterodyne focal plane detector, " in *Proc. 22nd Int. Symp. Space THz Techn.*, 2011, pp. 164-170.

[28] C. E. Groppi and J. H. Kawamura, "Coherent detector arrays for terahertz astrophysics applications," *IEEE Trans. THz Sci. Technol.*, vol. 1, no. 1, pp. 85-96, Sep. 2011.

[29] S. Paine, "Beam waveguide and receiver optics for the SMA," in *Proc. 5th Int. Symp. Space THz Techn.*, 1994, pp. 811-823.

[30] T. S. Chu, "An imaging beam waveguide feed," *IEEE Trans. Antennas Propag.*, vol. 31, no. 4, pp. 614-619, Jul. 1983.

[31] S. Paine (1995, May 7). *SMA optics* [Online]. Available: http://www.cfa.harvard.edu/sma/private/eng_pool/spaine/proj_book_optics/proj_book_optics.html

[32] P. F. Goldsmith, "Gaussian Beam Transformation," in *Quasioptical systems: Gaussian beam quasioptical propagation and applications*, 1st ed, Piscataway, NJ: IEEE Press, 1998, ch. 3, sec. 3.2-3.3, pp. 40-53.

[33] *Technical Description*, ver. 10.1.0, TICRA, Copenhagen, Denmark, 2008, pp. 122-212.

[34] A. C. Ludwig, "The definition of cross polarization", *IEEE Trans. Antennas Propag.*, vol. 21, pp. 116-119, Jan. 1973.

[35] *Technical Description*, ver. 10.1.0, TICRA, Copenhagen, Denmark, 2008, pp. 245.

[36] *Technical Description*, ver. 10.1.0, TICRA, Copenhagen, Denmark, 2008, pp. 142.

[37] L. Olmi, "The optical design of relay optics for heterodyne millimeter wave focal plane array," *Int. Jour. Infr. Mm. Waves*, vol. 21, No. 3, pp. 365-393, 2000.